AD-A108 577 PACIFIC-SIERRA RESEARCH CORP SANTA MONICA CA F/G 4/1
CALCULATION OF IONOSPHERIC CONDUCTIVITY PROFILES BY INVERTING V--ETC(U)
OCT 81 R E WARREN, E C FIELD, C R WARBER F19628-78-C-0088
UNCLASSIFIED PSR-1114 RADC-TR-81-286 NL

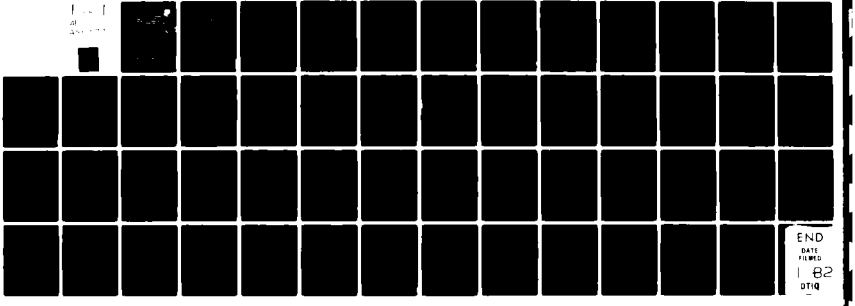

END
DATE FILMED
1-82
DTIC

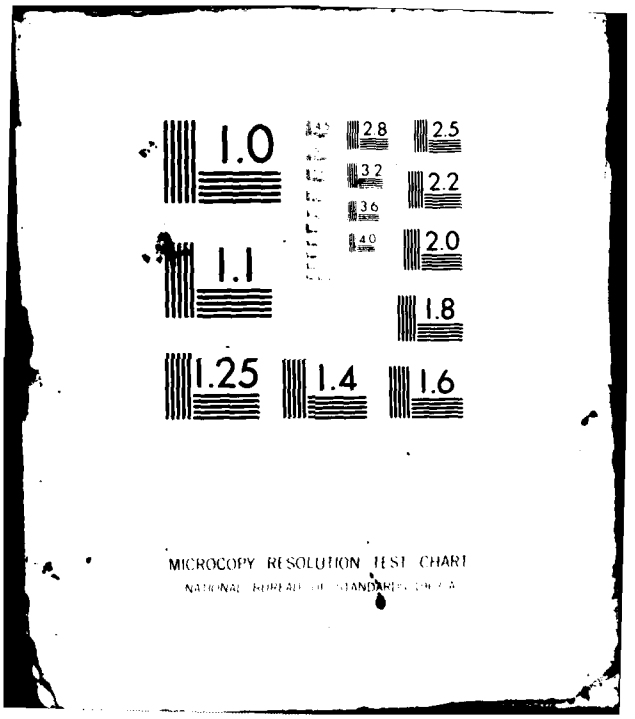
1.0
1.1
1.25
1.4
1.6
2.8
3.2
3.6
4.0
2.5
2.2
2.0
1.8
MICROCOPY RESOLUTION TEST CHART

RADC-TR-81-286
Final Technical Report
October 1981

CALCULATION OF IONOSPHERIC CONDUCTIVITY PROFILES BY INVERTING VLF/LF REFLECTION DATA: I. ISOTROPIC PROPAGATION

Pacific-Sierra Research Corp.

R. E. Warren
E. C. Field
C. R. Warber

ROME AIR DEVELOPMENT CENTER
Air Force Systems Command
Griffiss Air Force Base, New York 13441

This report has been reviewed by the RADC Public Affairs Office (PA) and is releasable to the National Technical Information Service (NTIS). At NTIS it will be releasable to the general public, including foreign nations.

RADC-TR-81-286 has been reviewed and is approved for publication.

APPROVED: Terrence J. Elkins

TERRENCE J. ELKINS
Chief, Propagation Branch
Electromagnetic Sciences Division

APPROVED: Allan C. Schell

ALLAN C. SCHELL
Chief, Electromagnetic Sciences Division

FOR THE COMMANDER: John P. Huss

JOHN P. HUSS
Acting Chief, Plans Office

If your address has changed or if you wish to be removed from the RADC mailing list, or if the addressee is no longer employed by your organization, please notify RADC (EEPL) Hanscom AFB MA 01731. This will assist us in maintaining a current mailing list.

Do not return copies of this report unless contractual obligations or notices on a specific document requires that it be returned.

UNCLASSIFIED

SECURITY CLASSIFICATION OF THIS PAGE (When Data Entered)

REPORT DOCUMENTATION PAGE		READ INSTRUCTIONS BEFORE COMPLETING FORM
1. REPORT NUMBER RADC-TR-81-286	2. GOVT ACCESSION NO.	3. RECIPIENT'S CATALOG NUMBER
4. TITLE (and Subtitle) CALCULATION OF IONOSPHERIC CONDUCTIVITY PROFILES BY INVERTING VLF/LF REFLECTION DATA: I. ISOTROPIC PROPAGATION		5. TYPE OF REPORT & PERIOD COVERED Final Technical Report Oct 79 - May 81
		6. PERFORMING ORG. REPORT NUMBER PSR Report 1114
7. AUTHOR(s) R. E. Warren E. C. Field C. R. Warber		8. CONTRACT OR GRANT NUMBER(s) F19628-78-C-0088
9. PERFORMING ORGANIZATION NAME AND ADDRESS Pacific-Sierra Research Corporation 1456 Cloverfield Blvd Santa Monica CA 90404		10. PROGRAM ELEMENT, PROJECT, TASK AREA & WORK UNIT NUMBERS 61102F 2304J322
11. CONTROLLING OFFICE NAME AND ADDRESS Deputy for Electronic Technology (RADC/EEP) Hanscom AFB MA 01731		12. REPORT DATE October 1981
		13. NUMBER OF PAGES 43
14. MONITORING AGENCY NAME & ADDRESS(if different from Controlling Office) Same		15. SECURITY CLASS. (of this report) UNCLASSIFIED
		15a. DECLASSIFICATION/DOWNGRADING SCHEDULE N/A

16. DISTRIBUTION STATEMENT (of this Report)

Approved for public release; distribution unlimited.

17. DISTRIBUTION STATEMENT (of the abstract entered in Block 20, if different from Report)

Same

18. SUPPLEMENTARY NOTES

RADC Project Engineer: Paul A. Kossey (EEP)

19. KEY WORDS (Continue on reverse side if necessary and identify by block number)

Lower Ionosphere
VLF/LF reflection
VLF/LF inverse problem
Ionosounding

20. ABSTRACT (Continue on reverse side if necessary and identify by block number)

This report presents an iterative method for inverting VLF/LF ionosounding data to obtain ionospheric conductivity profiles. The relationship between the detail that can be realized in the calculated profile and the quality and quantity of the reflection data is given explicitly. Only altitudes below about 70 km where the propagation can be assumed isotropic are considered, although the method can be extended to anisotropic propagation. The method is demonstrated by applying it

DD FORM 1 JAN 73 1473 EDITION OF 1 NOV 65 IS OBSOLETE

UNCLASSIFIED

SECURITY CLASSIFICATION OF THIS PAGE (When Data Entered)

to two qualitatively different ionospheric models--a strong SPE disturbance and a C-layer exhibiting a well-defined conductivity peak. Ground-level reflection data contain information only about those heights from which significant energy is returned. The calculated profiles agree well with the true profiles over the height range where the strongest reflections occur, and break down outside of that range. The solutions converge toward the true profiles despite the use of initial estimates that contain no information about the true ionospheric structure. The height resolution actually achieved for the two examples is much better than the theoretically predicted limit.

SUMMARY

This report presents an iterative method for inverting VLF/LF ionosound data to obtain ionospheric conductivity profiles. The relationship between the detail that can be realized in the calculated profile and the quality and quantity of the reflection data is given explicitly by our approach. We consider only altitudes below about 70 km where the propagation can be assumed isotropic, although the method can be extended to anisotropic propagation.

We demonstrate the method by applying it to two qualitatively different ionospheric models--a strong SPE disturbance and a C-layer exhibiting a well-defined conductivity peak. Ground-level reflection data contain information about only those heights from which significant energy is returned. Our calculated profiles agree well with the true profiles over the height range where the strongest reflections occur, and break down outside of this range. The solutions converge toward the true profiles despite our use of initial estimates that contain no information about the true ionospheric structure. The height resolution actually achieved for the two examples is much better than the theoretically predicted limit.

PREFACE

This report describes a method for inverting VLF/LF reflection data to obtain ionospheric conductivity profiles under conditions where the propagation can be assumed isotropic. We demonstrate the method by inverting computer-generated reflection coefficients for two generic model ionospheres. In addition, we present a means of choosing the best compromise between the deleterious effects of (1) noisy data and (2) loss of uniqueness due to incomplete data.

CONTENTS

FIGURES

TABLES

I. INTRODUCTION

Radio-sounding at VLF (3 to 30 kHz) and LF (30 to 300 kHz) is often used to sample the ionosphere at heights below about 100 km where high-frequency (HF) ionosounds provide little information. Further, at altitudes below about 70 km the electron density is often too small to be sensed by rocket-borne probes, and VLF/LF sounding is the only sampling means available. Once ground-level VLF/LF reflection coefficients have been measured, they must be inverted to infer ionospheric structure. This "inverse" problem is much more difficult than the "forward" problem of calculating reflection coefficients from a specified model ionosphere.

Inversion of ionosound data is often performed by trial and error, with reflection coefficients being calculated from a number of model ionospheres, and the model giving the coefficients that--in the judgment of the analyst--most closely agree with experiment being deemed correct. This report describes a method for inverting VLF/LF reflection data to obtain ionospheric conductivity profiles without using trial and error. We consider only altitudes below about 70 km where the propagation can be assumed isotropic, although the method can be extended to anisotropic propagation. This restriction on altitude limits the applicability to disturbed conditions--such as solar-proton events (SPE)--and some ambient daytime situations.

Our procedure extends the spectral method described by Parker [1977] for implementing the Backus and Gilbert theory [1967, 1968, 1970, 1971], which was developed for inverting seismic or electromagnetic soundings of the earth's interior. We find that method to be well suited to the ionosphere as well. Chuang and Yeh [1977] applied the Backus and Gilbert theory to HF ionosound data. However, they used geometric optics, whereas VLF/LF propagation must usually be described by full-wave theory. Shellman [1973] and Morfitt and Shellman [1977] inverted VLF/LF ionospheric reflection data, including geomagnetic anisotropy, by performing a least-squares optimization of the electron density and collision frequency. That approach, although

direct, requires that the number and location of the sampling heights be selected beforehand. The Backus-Gilbert method requires no such preselection and imposes fewer constraints on the functional form of the inverse solution. Moreover, it gives the relationship between the detail that can be realized in the calculated conductivity height profile and the quality and quantity of the reflection data.

Section II describes the mathematical basis of our inversion method. Section III applies the method to actual and computer-synthesized reflection-coefficient data and evaluates uncertainties in the inferred profiles caused by noise and incomplete data. Section III also presents a means of estimating the height range over which waves at the sounding frequencies interact strongly with the ionosphere; and, therefore, the height range over which the sounding data can provide information on ionospheric structure. Section IV gives the conclusions, and the Appendix presents certain mathematical details.

II. INVERSE THEORY APPLIED TO IONOSOUNDING DATA

Inferring ionospheric height profiles from ground-based reflection data is one of a class of problems treated by inverse theory, the object of which is to use limited and usually noisy data to determine the maximum information about geophysical structure. Inverse problems are typically much more difficult than forward problems, which require calculation of the signal emerging from specified propagation media. This difficulty is due primarily to the nonuniqueness of the inferred profile. Backus and Gilbert [1967] showed that--under fairly general conditions--a finite data set is consistent with an infinite number of possible profiles, if it is consistent with any one. In addition, in many cases (including the one addressed here), the measured signal has a nonlinear dependence on the propagation medium. This nonlinearity could introduce nonuniqueness, because the unknown profile must be constructed iteratively from a starting estimate and different starting estimates can, *in principle*, produce different profiles.

Despite these difficulties, the importance of obtaining information about the earth or its environment from remote probes has led to at least a partial resolution of questions pertaining to uniqueness [Backus and Gilbert, 1967, 1968, 1970; Oldenburg, 1978]. The nonuniqueness due to incomplete data is fairly well understood and characterized. That due to nonlinear dependence on the medium is still unresolved, but seems to cause no difficulty for the numerical examples that we give in Sec. III.

FRÉCHET KERNELS FOR ISOTROPIC IONOSPHERIC CONDUCTIVITY

The first step in the inverse solution is to characterize the dependence of the reflection coefficients on the structure of the ionosphere. For TM (vertically polarized) waves the reflection coefficient R below the ionosphere can be defined as

$$R = H_y^{(d)} \Big/ H_y^{(u)} , \qquad (1)$$

where $H_y^{(u)}$ and $H_y^{(d)}$ are incident and reflected magnetic intensities measured at the same point, and y is the cartesian coordinate normal to the plane of incidence. The equation governing R for plane waves reflected from an isotropic ionosphere is [Budden, 1961]

$$\frac{2i}{k}\frac{dR}{dz} = Cn^2(1 - R)^2 - \frac{q^2}{n^2C}(1 + R)^2 , \tag{2}$$

where n(z) is the complex refractive index, $q^2 = n^2 - S^2$, S and C are the sine and cosine of the incident wave in free space, and k is the free-space wave number. An analogous equation exists for the TE (horizontally polarized) reflection coefficient [Budden, 1961], but we will consider only vertically polarized waves.

The general refractive index expression, including geomagnetic effects, is

$$n^2 = 1 - \frac{e^2}{\omega\varepsilon_0}\sum_{\gamma}\frac{N_\gamma(z)}{m_\gamma(z)[\omega - i\nu_\gamma(z) \pm \omega_{C\gamma}(z)]} , \tag{3}$$

where the sum is over all charged species (electrons, positive and negative ions), ω is the angular frequency, e is the electronic charge, ε_0 is the permittivity of free space, and N_γ, m_γ, ν_γ, and $\omega_{C\gamma}$ are the height-dependent number density, mass, collision frequency, and gyrofrequency of the γth species. The isotropic equation (2) is valid provided all important reflections occur below altitudes of 70 to 75 km, where $\nu > \omega_C$. Moreover, since $\omega << \omega_C < \nu$ at VLF/LF in this low-altitude regime, n^2 assumes the simplified form

$$n^2(z) \simeq 1 - i\frac{\sigma(z)}{\omega\varepsilon_0} , \tag{4}$$

where the total conductivity is given by

$$\sigma(z) \simeq e^2\sum_{\gamma}\frac{N_\gamma}{m_\gamma\nu_\gamma} . \tag{5}$$

Heavy ions make important contributions to the conductivity only at altitudes below 50 to 55 km above which the conductivity may be considered entirely due to electrons. At altitudes where Eqs. (2) and (4) are valid, reflection data can provide information only about the total conductivity. Auxiliary information is needed to separate the components appearing in Eq. (5).

Equation (2)--with n^2 given by Eq. (4)--can be integrated numerically for a given ω to obtain R(0) at the ground. We start the integration from the initial estimate

$$R(z_m) = \frac{n^2C - q}{n^2C + q} , \qquad (6)$$

where z_m is chosen large enough for R to be slowly varying, and Eq. (6) results from setting dR/dz = 0 in Eq. (2). This solution for the reflection coefficient R(0), corresponding to a given conductivity profile $\sigma(z)$, comprises the forward problem.

The inverse problem is to obtain the best possible estimate of $\sigma(z)$ from R(0), specified at a finite set of frequencies. We construct σ by computing successive corrections to an initial estimate $\sigma^0(z)$, each correction being determined by relating a small change $\delta\sigma(z)$ in conductivity at height z to a change $\delta R_i(0)$ in the ground-level reflection coefficient at frequency $f_i = \omega_i/2\pi$. We find the necessary relationship by expanding an equation analogous to Eq. (2) for $R'(z) = R(z) + \delta R(z)$ in terms of $\sigma'(z) = \sigma(z) + \delta\sigma(z)$, retaining only terms linear in δR and $\delta\sigma$, and using Eq. (2). The resulting linear first-order differential equation for $\delta R(z)$ is

$$\frac{d}{dz}\,\delta R + P(z)\delta R(z) = Q(z) , \qquad (7)$$

where

$$P(z) = \frac{k}{i}\left[Cn^2(1 - R) + \frac{q^2}{n^2C}(1 + R)\right] , \qquad (8)$$

$$Q(z) = -\frac{1}{2}\sqrt{\frac{\mu_0}{\varepsilon_0}}\left[C(1-R)^2 - \frac{S^2}{n^4 C}(1+R)^2\right]\delta\sigma(z) \ . \qquad (9)$$

Equation (7) can be integrated to give

$$\delta R(0) = -\int_0^{z_m} dz\, Q(z)\, \exp\left[\int_0^z dz'\, P(z')\right]$$

$$+ \delta R(z_m)\, \exp\left[\int_0^{z_m} dz\, P(z)\right] \ . \qquad (10)$$

P contains a negative real component; so the second term is negligible at the ground, and

$$\delta R(0) \simeq \int_0^{z_m} dz\, G(z)\delta\sigma(z) \ , \qquad (11)$$

where C is the Fréchet kernel, which relates a small change in conductivity at altitude z to a change in reflection coefficient at the ground:

$$G(z) = \frac{1}{2}\sqrt{\frac{\mu_0}{\varepsilon_0}}\left[C(1-R)^2 - \frac{S^2}{n^4 C}(1+R)^2\right]$$

$$\times \exp\left\{\frac{k}{i}\int_0^z dz'\left[Cn^2(1-R) + \frac{q^2}{n^2 C}(1+R)\right]\right\} \ . \qquad (12)$$

CONSTRUCTION OF THE INVERSE SOLUTION

As emphasized by Backus and Gilbert [1967, 1968, 1970], the estimation of an unknown propagation medium from a finite set of field measurements requires two steps. First, we must construct a conductivity profile that reproduces the data. Second, and equally important, we must characterize the class of solutions to which our profile and--presumably--the true profile belong. Here we address the first step. The uniqueness of our inverse solution is considered in the following subsection.

To construct the inverse solution we must find a conductivity profile that matches a set of reflection coefficient data at a number (n) of frequencies. Following Oldenburg [1978], we pick an initial estimate σ^0, compute R_i^0 from Eq. (2) at each frequency f_i, and set

$$\delta R_i^1 = R_i^{data} - R_i^0(0) , \qquad i = 1, \ldots, n , \tag{13}$$

where superscripts denote the order of the correction (i.e., the number of iterations), and subscripts index the frequencies. We then express the first-order correction to σ^0, $\delta\sigma^1$, as

$$\delta\sigma^1(z) = \sum_{j=1}^{n} \alpha_j G_j^*(z) , \tag{14}$$

where the α_j are found by solving the $n \times n$ set of equations

$$\sum_{j=1}^{n} \Gamma_{ij}\alpha_j = \delta R_i^1 \tag{15}$$

and

$$\Gamma_{ij} = \int_0^{z_m} dz\, G_i(z)G_j^*(z) . \tag{16}$$

Next, R_i^1 is computed from Eq. (2) using the new conductivity estimate $\sigma^1(z) = \sigma^0(z) + \delta\sigma^1(z)$, and the process is successively repeated. At each iteration N we use the rms relative error

$$\varepsilon^N = \left(\frac{1}{n} \sum_{i=1}^{n} \left| \delta R_i^N / R_i^{data} \right|^2 \right)^{1/2} \tag{17}$$

as a measure of convergence.

In practice, we use tne following modifications to the above procedure:

1. Because the data and Fréchet kernels are expressed in complex form, the differential conductivities $\delta\sigma^i$ produced by Eq. (14) can have imaginary parts. We have found it sufficient to use the fact that the conductivity in Eq. (14) must be real and simply suppress the imaginary part of the correction at each iteration. A more rigorous--and complicated--approach would be to express all quantities in real form at the outset.
2. As discussed by Oldenburg, direct use of the output corrections to the conductivity at each iteration tends to produce oscillatory profiles, and a nonphysical build-up of conductivity at low heights. These pathologies require that each correction be substantially smoothed and filtered before being used in the next iteration. In addition, we do not allow the total conductivity at any iteration to become negative but redefine it as zero, if required, before proceeding. These steps slow the convergence, but appear necessary to produce realistic profiles.
3. Following Parker [1977] we diagonalize the matrix Γ before inversion, so the expansion [Eq. (14)] is actually performed in the eigenfunctions of the Γ matrix. This step allows each term in the diagonalized basis to be associated with a

relative uncertainty in the data, and components that introduce large statistical uncertainties can be omitted. The Appendix gives the details of this spectral expansion method.

UNIQUENESS OF THE INVERSE SOLUTION

The above algorithm is iterated until the relative rms error [Eq. (17)] asymptotically approaches a minimum. We have then done as well as possible in constructing a conductivity profile with the data and starting estimate used. The remaining task is to assess the validity of the profile at various heights. As discussed above there are three sources of nonuniqueness:

1. Noise in the reflection coefficient data causes uncertainties.
2. The data set is finite, and therefore incomplete.
3. The conductivity profile and reflection coefficient data are nonlinearly related.

The first error source is easily assessed with multivariate error analysis. The spectral expansion method (see Appendix) provides a simple means of estimating the effect of measurement uncertainties on the accuracy of the inferred conductivity profile. More important, variances in the reflection data are included in the solution in a manner that deemphasizes frequencies at which measurements are exceptionally noisy.

The second type of nonuniqueness has received the most attention in the literature, since it is present regardless of the care taken to reduce experimental uncertainty. It is therefore the ultimate limitation on using a finite data set to characterize an unknown function. Before specifically addressing this type of nonuniqueness, we consider a somewhat similar situation, which is helpful in understanding inaccuracies caused by incomplete data.

The Fourier series representation of an arbitrary periodic function $\phi(x)$, $0 < x < 2\pi$, is given by

$$\phi(x) = \frac{1}{\sqrt{2\pi}} \sum_{n=-\infty}^{\infty} C_n \, e^{inx} \, , \tag{18a}$$

where

$$C_n = \frac{1}{\sqrt{2\pi}} \int_0^{2\pi} dx \; \phi(x) \; e^{-inx} \, . \tag{18b}$$

It is well known that--subject to some weak requirements--the *infinite* set of coefficients $\{C_n\}$ completely defines ϕ. If, however, only a *finite* set $-N \leq n \leq N$ of Fourier coefficients is given, the high-frequency content of ϕ will be lost; and any ϕ' that differs from ϕ only in these neglected components will have the same coefficients C_n, for $|n| \leq N$.

To quantify the uncertainty caused by omitting the coefficients of index $|n| > N$, we let $\langle\phi\rangle$ denote the estimate for ϕ based on the incomplete set of C_n, and write

$$\langle\phi(x)\rangle = \frac{1}{\sqrt{2\pi}} \sum_{n=-N}^{N} C_n \, e^{inx} \, . \tag{19}$$

By using Eq. (18b), we find

$$\langle\phi(x)\rangle = \int_0^{2\pi} dx' \; \phi(x') A_N(x, x') \, , \tag{20a}$$

where

$$A_N(x, x') = \frac{1}{2\pi} \sum_{n=-N}^{N} e^{in(x-x')} \, . \tag{20b}$$

A_N is the Dirichlet kernel, and is a measure of how closely ϕ can be resolved by the finite harmonic set. The width of A_N is proportional to 1/N, so the resolution improves as the number of "data" points becomes larger. In the limit $N \to \infty$, $\langle\phi\rangle \to \phi$, and the resolution becomes perfect. This behavior occurs because A_N approaches a Dirac delta function for large N.

The above approach can be used in the ionospheric inverse problem to quantify the loss of resolution due to having incomplete reflection data. For a given iteration, Eq. (14) can be written

$$\langle\delta\sigma(z)\rangle = \sum_{j=1}^{n} \alpha_j G_j^*(z) \ , \tag{21}$$

where we place $\langle\ \rangle$ around $\delta\sigma$ to emphasize that only a finite set of frequencies is available, and our estimate can therefore differ from the "true" correction $\delta\sigma$. By using Eqs. (15) and (11), we find

$$\alpha_j = \sum_{k=1}^{n} \Gamma_{jk}^{-1} \, \delta R_k(0)$$

$$= \sum_{k=1}^{n} \Gamma_{jk}^{-1} \int_0^{z_m} dz' \ G_k(z')\delta\sigma(z') \tag{22}$$

and substitution into Eq. (21) gives

$$\langle\delta\sigma(z)\rangle = \int_0^{z_m} dz' \ \delta\sigma(z')A(z, z') \ , \tag{23}$$

with

$$A(z, z') = \sum_{j,k=1}^{n} \Gamma^{-1}_{jk} G^*_j(z) G_k(z') \ . \qquad (24)$$

The averaging function [Eq. (24)] is the analog of the Dirichlet kernel for Fourier series. Variations of the conductivity on a scale shorter than the width of $A(z, z')$ about a given height will not be resolvable by the data set used to generate the profile. Even though we constructed the averaging function for a small variation in conductivity, Backus and Gilbert [1968] prove that--to order $|\delta\sigma(z)|^2$--Eq. (24) provides a measure of the height resolution of the total conductivity.

We show in the Appendix that Eq. (24) can be rewritten in essentially the form

$$A(z, z') = \sum_{i=1}^{k\leq n} H^*_i(z) H_i(z') \ , \qquad (25)$$

where the functions $H_i(z)$ are produced by orthonormalizing the set of Fréchet kernels $G_i(z)$. As for the orthonormal Fourier series basis function discussed above, the H_i functions can be ranked in order of increasingly oscillatory behavior. The diagonal form of the averaging function given by Eq. (25) is convenient for evaluating the importance of retaining the more oscillatory components. In general, a better fit to the data is achieved by increasing the number of components used in the construction of $\delta\sigma(z)$. However, the resulting conductivity profile can exhibit nonphysical oscillations if too many terms are retained.† The optimum number of components H_i depends partly on the estimated noise in the data, and partly on the analyst's intuition regarding profile smoothness. The relation of resolution

†This situation is analogous to that which can be encountered in fitting a high-order polynomial to a large number of data points. The polynomial can match the data exactly at each point, but exhibit spurious oscillations between the points.

to noise is treated in the next section and the Appendix. Its relation to the analyst's intuition is difficult to quantify, however.

The remaining source of nonuniqueness is the nonlinear relation between conductivity and the ground-level reflection coefficient. This source is by far the most difficult to characterize in general, because there is no guarantee that other "globally" different conductivity profiles would not be obtained with different initial estimates σ^0. The most practical means of exploring this possibility is to choose widely different starting estimates and see if the calculated profiles agree, aside from minor variations. We have found that our algorithm produces iterative solutions even with a null initial estimate ($\sigma^0 = 0$). Moreover, calculations made from the same data sets--but with various nonzero estimates--gave virtually identical profiles. These results strongly suggest (but do not prove) that--in practice--the nonlinear dependence of the reflection coefficients on ionospheric structure causes no loss of uniqueness.

III. NUMERICAL EXAMPLES

This section applies the inversion method developed in Sec. II and the Appendix. Recall that our assumption of isotropic propagation restricts this application to conditions where all important reflections occur below 70 to 75 km. We use the examples given below to test the ability of our inversion method to obtain correct conductivity height profiles from a set of ground-level reflection coefficients; and to assess the effects of measurement noise and incomplete data on the accuracy and height resolution of our results. The examples were chosen to illustrate the salient aspects of our approach and are intentionally simple. Our method should work equally well for more complicated situations.

STRONG SPE

Our first example is based on high-latitude satellite measurements of incident particle fluxes at 1508 UT time on 4 August 1972. These measurements were made near the peak of one of the strongest SPEs on record. Height profiles of electron and ion densities were calculated from the measured fluxes with Lockheed's air-chemistry code, and provided to the authors by Reagan [1978]. These densities, along with nominal height profiles of electron and ion collision frequencies and masses were used with Eq. (5) to obtain the conductivity height profile shown (solid line) in Fig. 1. This profile is an example of an extremely severe natural disturbance.

Here we illustrate application of our method rather than perform detailed calculations for specific situations. Therefore, for convenience, we approximate the strong SPE profile with the often-used form

$$\sigma(z) = \sigma_0 \, e^{\beta z} \, , \tag{26}$$

where $\sigma_0 = 3.94 \times 10^{-15}$ mhos/m and $\beta = 0.39$ km^{-1}. Figure 1 shows the agreement between the approximation [Eq. (26)] and the actual conductivity profile.

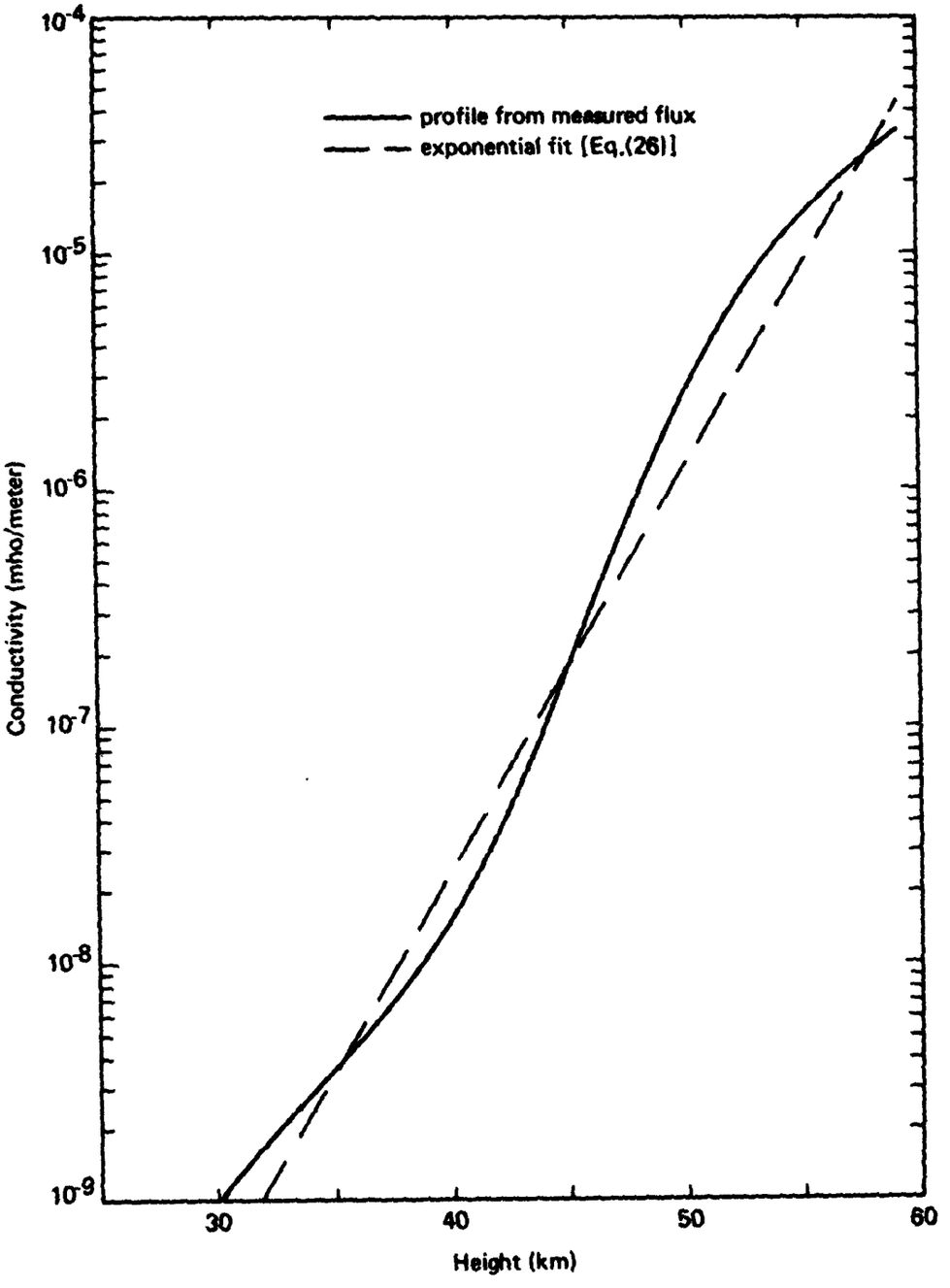

Fig. 1--Conductivity height profile for a strong SPE

Inverse Solution

To provide a starting point for our inverse solution, we have calculated TM reflection coefficients for the profile given by Eq. (26) by integrating Eq. (2) for an incidence angle of 65 deg at frequencies of 4, 6, 9, 14, 21, 30, and 48 kHz. Our reason for choosing this set of frequencies is discussed below. These coefficients serve as artificial "data," which are analogous to measured data that would be available from ionosounders. To suppress the unphysical build-up of conductivity below 35 km, we use the weighting technique of Oldenburg [1978] (see Appendix), and choose

$$w(z) = \begin{cases} 0 , & z \le b \\ 1 - \exp\left[-\gamma(z - b)\right] , & z \ge b \end{cases} \tag{27}$$

for the weighting function w(z) with b = 35 km, $\gamma = 0.5\ \text{km}^{-1}$. We compute successive corrections to the conductivity using the spectral expansion method and a null ($\sigma^0 = 0$) starting estimate. Therefore, our initial profile contains no information about the true profile. Oscillations in the corrections $\delta\sigma$ for each iteration are controlled by our use of a weighted average of the correction at height z (weight 0.5) and at 0.7 km above and below z (weight 0.25).

Figure 2 shows the computed conductivity profile following the $1st$, $5th$, $10th$, and $15th$ iterations, the true profile (dashed lines), and the relative rms error ϵ. The computed profile was still slowly increasing near 50 km after the $15th$ iteration, and more iterations presumably would have given closer agreement with the true profile between 49 and 50 km. Figure 3 gives an expanded plot of the calculated and true profiles after the $15th$ iteration. The agreement is good at altitudes between about 40 and 49 km. Outside of this altitude range the calculated conductivity is much smaller than the true conductivity. We give the physical reason for this disagreement below.

Sensitivity to Noise and Limited Data

To evaluate the effect of measurement noise on the inferred conductivity, we include hypothetical uncertainties S_i in the reflection

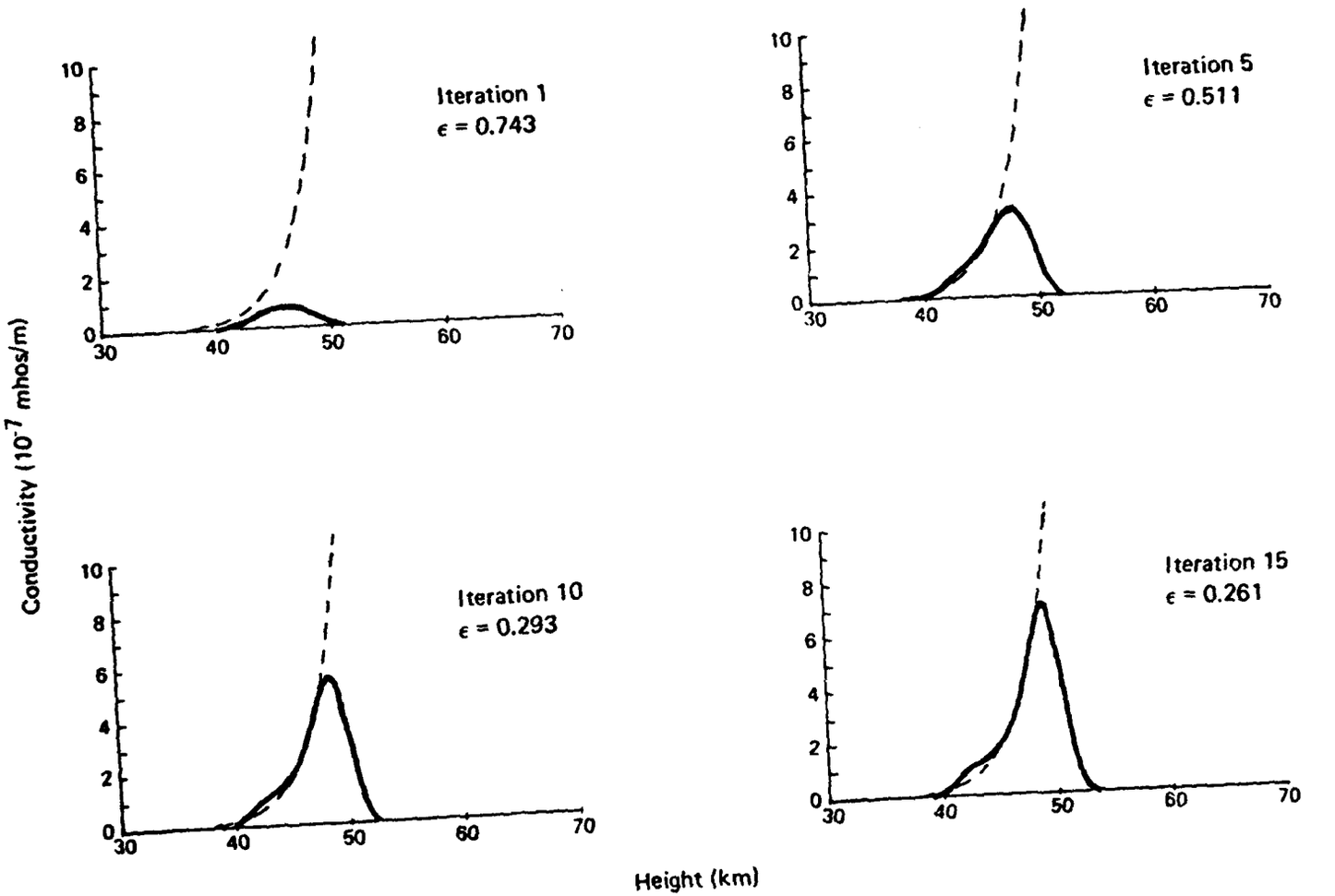

Fig. 2--Calculated conductivity profiles (solid curves) and true profile (dashed curve) for the strong SPE example

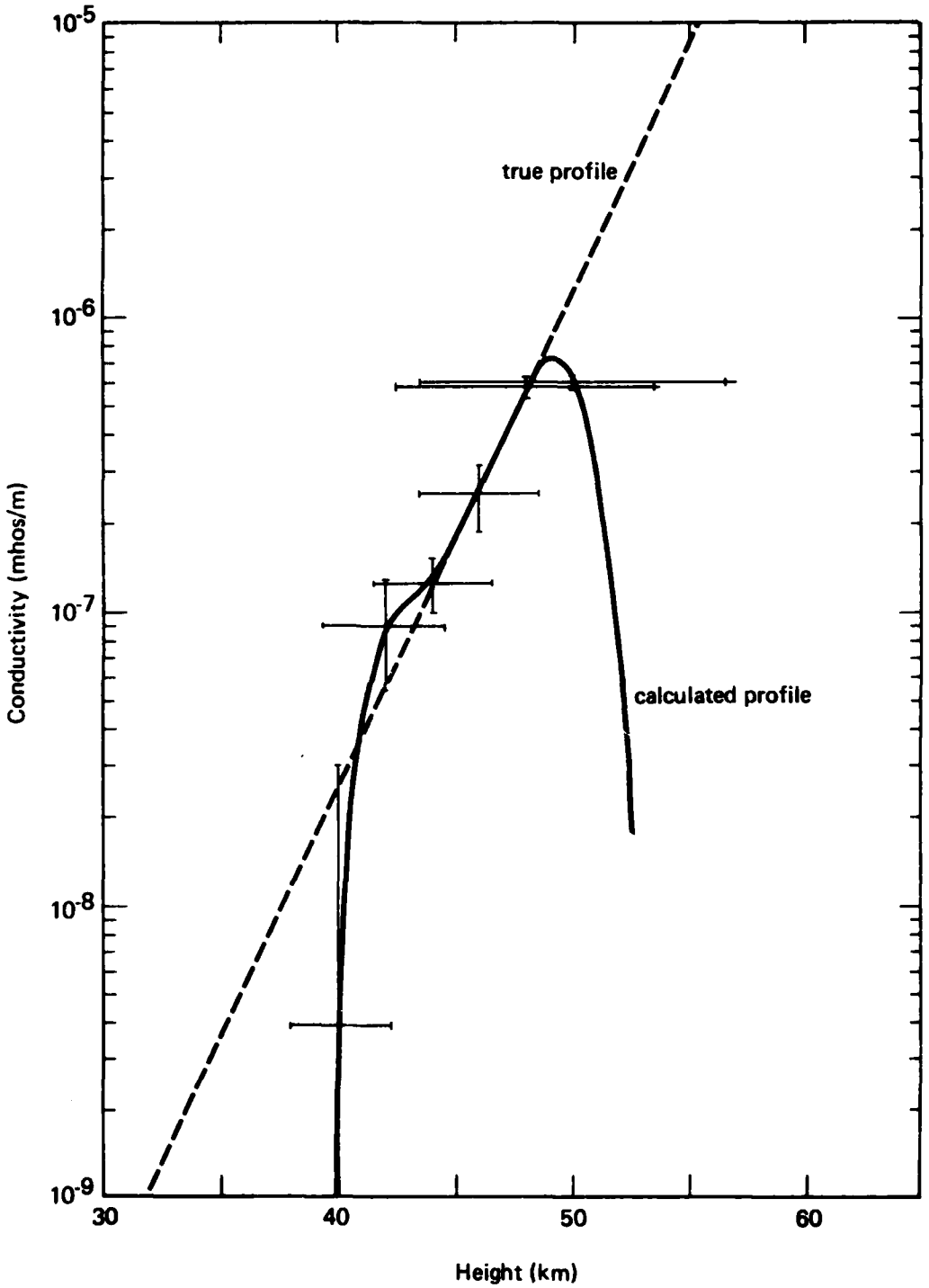

Fig. 3--Calculated and true profiles after 15 iterations for the strong SPE example. Vertical bars show uncertainty caused by hypothetical noise in the reflection coefficients. Horizontal bars show uncertainty caused by incompleteness of the reflection data.

coefficients used in our calculations. The values for S_i are derived from typical measurement uncertainties (Rasmussen [1981]) and are listed in Table 1.

Table 1

ASSUMED UNCERTAINTIES IN REFLECTION COEFFICIENTS FOR THE STRONG SPE EXAMPLE

Frequency (kHz)	$\lvert S_i/R_i(0)\rvert$
4	0.3
6	0.3
9	0.3
14	0.25
21	0.1
30	0.1
48	0.15

By including S_i, we can examine sensitivity of the profile at various heights to measurement noise, even though the computer-generated "data" are noiseless.

The variance in conductivity is defined as

$$\text{Var}\,[\sigma(z)] \equiv \langle\sigma^2(z)\rangle - \langle\sigma(z)\rangle^2 \,, \tag{28}$$

where $\langle\ \rangle$ denotes averages. The Appendix shows that

$$\text{Var}\,[\sigma(z)] = [w(z)]^2 \sum_{i=1}^{k\le n} \frac{1}{\lambda_i} \lvert H_i(z)\rvert^2 \,, \tag{29}$$

where the sum is over the positive-definite contributions from each diagonalized component $H_i(z)$. The eigenvalues λ_i for the 15*th* iteration are listed in Table 2, as is the estimated variance at height 44 km formed by truncating Eq. (29) at different values of k. Table 2 shows that retention of fewer terms in Eq. (29) causes a decreased

Table 2

EFFECTS OF NOISE FOR STRONG SPE EXAMPLE

Eigenvalue		Cumulative $[\mathrm{Var}\ (\sigma)]^{1/2}$ (mhos/m)	
i = 1	1.81×10^{-6}	k = 1	1.70×10^{-9}
i = 2	4.32×10^{-7}	k = 2	3.89×10^{-9}
i = 3	9.46×10^{-9}	k = 3	1.69×10^{-8}
i = 4	1.72×10^{-9}	k = 4	2.38×10^{-8}
i = 5	4.51×10^{-10}	k = 5	9.19×10^{-8}
i = 6	1.95×10^{-11}	k = 6	2.35×10^{-7}
i = 7	2.65×10^{-13}	k = 7	5.40×10^{-6}

variance.* If variance were the only consideration, retention of only the first spectral component would provide the "best" solution. However, as discussed below, there is a tradeoff between noise variance and height resolution, and the solution retaining only i = 1 would provide poor resolution.

We evaluate resolution of the inferred profile by the generalized Dirichlet kernel method described in Sec. II and the Appendix. As for the variance, the achievable height resolution depends on the number of spectral components retained. Figure 4 shows the modulus of the averaging function A at height 44 km formed by truncating the Dirichlet representation |Eq. (25)| at various values of k. The best resolution--i.e., the narrowest averaging function--is achieved by retaining all seven terms. Unfortunately, as discussed above, the variance increases with the number of terms retained, and a compromise is needed.

Figure 5 illustrates the tradeoff between resolution and noise-induced variance in the conductivity height profile computed for the strong SPE. The resolution--defined as the full width at half-peak

*This behavior occurs because higher-order terms tend to be oscillatory and, therefore, exhibit a larger variance.

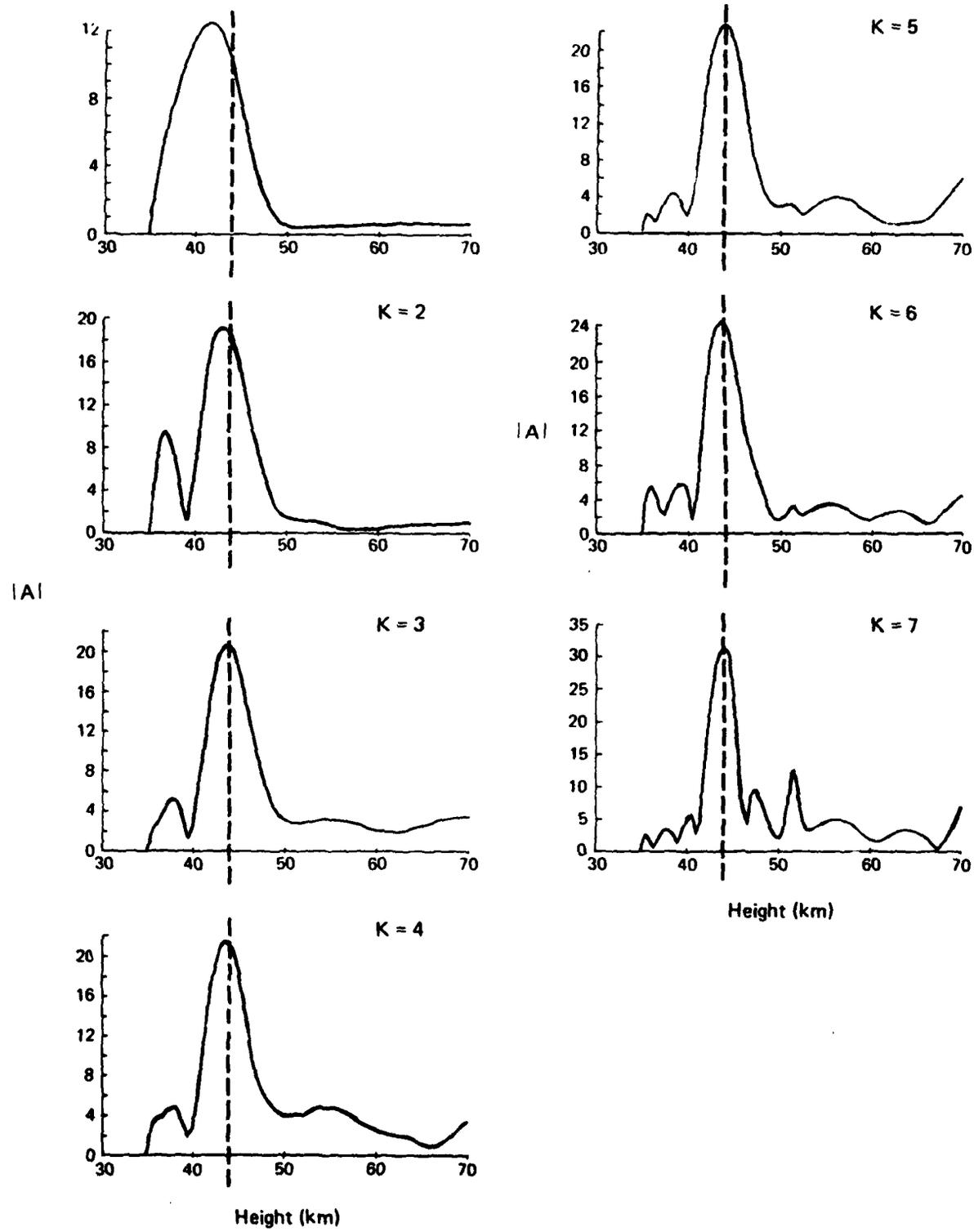

Fig. 4--Magnitude of the averaging function A for the strong SPE example (height = 44 km)

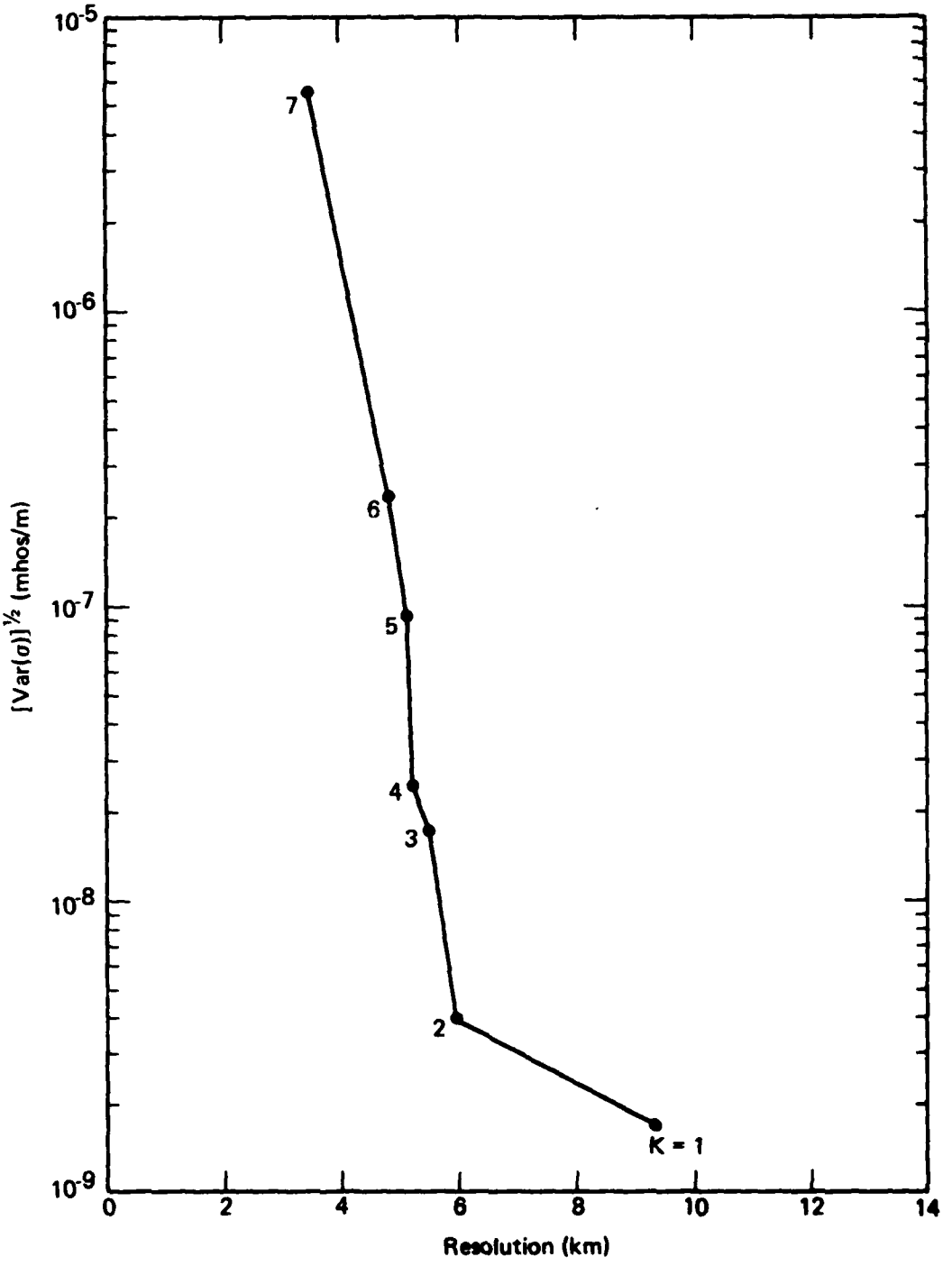

Fig. 5--Tradeoff between height resolution and noise-induced variance for the strong SPE example

of A--decreases as the number k of retained terms is increased, but at the expense of a greater variance. The vertical and horizontal bars in Fig. 3 show the resolution and $[\mathrm{Var}\ (\sigma)]^{1/2}$, respectively for k = 5, which we chose as a good compromise. If we had retained the maximum number of terms (k = n = 7), the resolution would improve from 5.1 to 3.5 km, but $[\mathrm{Var}\ (\sigma)]^{1/2}$ would increase by nearly two orders of magnitude. The optimum number of terms depends on the number of frequencies at which reflection data are available, and the amount of measurement noise. All terms (k = n) should be retained if noise is negligible, but only a few retained if the data are noisy. The optimum value for k must be selected on a case-by-case basis, using tradeoff graphs such as Fig. 5.

Physical Interpretation

We next show physically why the calculated profile shown in Fig. 3 agrees with the true profile only at heights between about 40 and 50 km. In addition, we give diagnostic methods for estimating the height range over which a set of reflection data can yield accurate conductivity profiles.

Ground-level reflection coefficients contain information about only those heights from which significant energy is returned. To estimate the heights at which important interactions between the incident field and the ionosphere occur, we use the following approximate expression (Field and Lewinstein [1978]) for the TM reflection coefficient:

$$R(0) = -\int_0^\infty dz \left[\frac{1}{2Q(z)}\frac{dQ}{dz}\right] \exp\left[-i2\omega\phi(z)/c\right] , \tag{30}$$

where

$$\phi(z) = \int_0^z dz'\, q(z') , \tag{31}$$

and $Q = q/n^2$. Equation (30) is the second-order WKB approximation, and is strictly valid only for weak reflections. Nonetheless, we will show that it provides useful insight into the reflection process. The integrand $\mathcal{R}$ of Eq. (30) is the contribution of a thin stratum at height z to the ground-level reflection coefficient. The quantity in brackets represents conversion of upgoing to downgoing waves in the stratum; the exponential term represents the round-trip transmission loss suffered in propagating to and from height z.

If we set

$$n^2(z) = 1 - i\alpha(z) \ , \tag{32}$$

the reflection-per-unit height $\mathcal{R}$ becomes

$$\mathcal{R}(z) = -\left\{\frac{i}{4}\frac{d\alpha}{dz}\frac{1 - 2C^2 + i\alpha}{(1 - i\alpha)(C^2 - i\alpha)} \exp\left[-i2\omega\phi(z)/c\right]\right\} , \tag{33}$$

which has magnitude

$$|\mathcal{R}(z)| = \frac{1}{4}\left\{\frac{d\alpha}{dz}\frac{1}{\left(C^4 + \alpha^2\right)^{1/2}}\left[1 - \frac{4C^2S^2}{1 + \alpha^2}\right]^{1/2}\right\} \exp\left[2\omega \mathrm{Im}\ \phi(z)/c\right] , \tag{34}$$

where

$$\mathrm{Im}\ \phi(z) = -\frac{1}{\sqrt{2}}\int_0^z \sqrt{\left(C^4 + \alpha^2\right)^{1/2} - C^2}\ dz' \ . \tag{35}$$

Figure 6 plots $|\mathcal{R}|$ for the exponential conductivity profile given by Eq. (26) at the frequencies used in the inversion, and Table 3 summarizes information from the figure. The quantity z_R denotes the height at which $|\mathcal{R}|$ attains its maximum value, and z_B and z_T denote heights below and above z_R, respectively, where $|\mathcal{R}|$ is one-half its peak value.

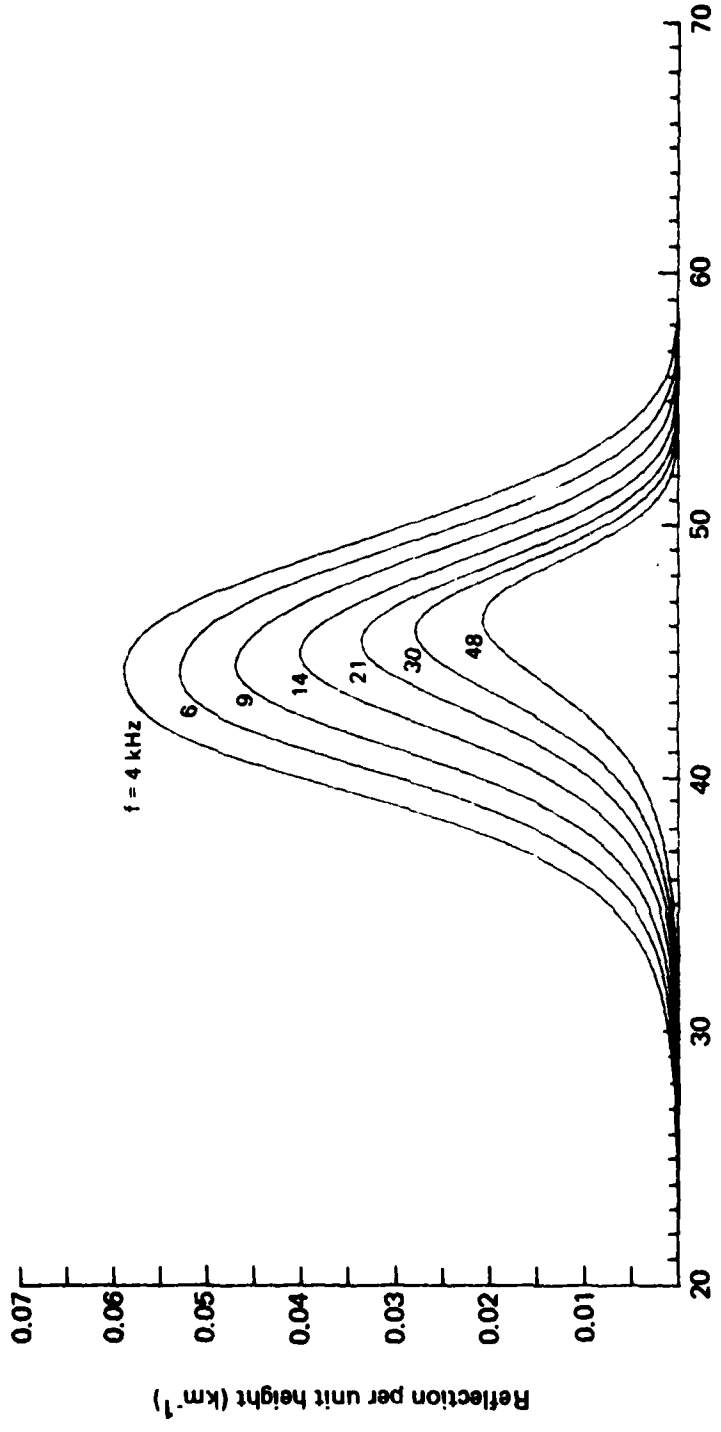

Fig. 6--Reflection per unit height for the strong SPE example

Table 3

REFLECTION REGIONS FOR STRONG SPE EXAMPLE

Frequency (kHz)	z_R (km)	z_B (km)	z_T (km)	Width ($z_T - z_B$) (km)
4	44.1	38.8	50.0	11.2
6	44.1	39.6	49.6	10.0
9	44.4	40.3	49.3	9.0
14	44.8	41.1	49.1	8.0
21	45.5	41.7	49.0	7.2
30	45.8	42.2	49.0	6.7
48	46.2	42.7	49.0	6.3

The maximum contribution to the ground-level reflection coefficient comes from heights near z_R, whereas relatively little contribution comes from heights below z_B or above z_T. Therefore, we expect the ground-level reflection coefficient to provide the best information on ionospheric conductivity in the height range bounded by z_B and z_T, and only poor information outside of this range.

Table 3 shows that z_R is a slowly increasing function of frequency, but remains near the center of the 40 to 50 km height range over the entire band considered. The lower height z_B increases from 39 to 43 km as the frequency is raised from 4 to 48 kHz, but the upper height z_T remains between 49 and 50 km. From Table 3 and Fig. 6 we conclude that, for the frequencies used, the reflection coefficients give little information about heights below 40 or above 50 km; and, even within the 40 to 50 km height range, the information is concentrated between about 44 and 50 km. This conclusion is consistent with Fig. 3, which shows excellent agreement between the calculated and true profiles between 44 and 49 km; fair agreement between 40 and 44 km; and a total breakdown below 40 or above 50 km.

The insensitivity of z_T to frequency indicates that the height range sampled by VLF/LF sounding could not be expanded substantially by using higher frequencies; and the use of frequencies much lower than 4 kHz is probably not practical. Thus, for the strong SPE example, VLF/LF sounding would appear incapable of determining the

state of the ionosphere below 40 or above 50 km. Finally, the fact that z_T is much lower than 70 km provides a posteriori justification of our neglect of geomagnetic effects.

Spacing of Frequencies

We have found that the best results are obtained by choosing an unequal spacing for the frequencies used. On physical grounds we expect that the optimum choice of frequencies would correspond to a uniform spacing of the heights of peak reflection z_R. We therefore need a mapping between reflection height and frequency. Unfortunately, Eq. (34) is inconvenient for this purpose. However, Field and Engel [1965] showed that--subject to certain restrictions--the major reflections take place within a few kilometers of the altitude where

$$\alpha = \sqrt{2}\, c^2 \ . \tag{36}$$

Specifically, by examining the second-order correction to the WKB approximation, they showed that substantial reflection can occur only at altitudes where

$$\left| \frac{\alpha}{q^3} \left(1 - \frac{2q^2}{n^2} \right) \right| \geq \frac{2k}{\beta} \ , \tag{37}$$

where we have used Eq. (26). Provided that $q^2 << n^2$, the peak value of the left side of Eq. (37) is easily shown to occur at the height where α is given by Eq. (36). By using Eqs. (4), (25), (32), and (37), we find

$$z_R \approx \frac{1}{\beta} \ell n \left[\sqrt{2}\, c^2 \frac{2\pi f \epsilon_0}{\sigma(0)} \right] \ . \tag{38}$$

Table 4 shows the values of z_R given by Eq. (38) for the strong SPE example. Note that the logarithmically-spaced frequencies correspond to evenly-spaced reflection heights. The differences between the approximate z_R in Table 4 and the more accurate ones in Table 3 do not appear to strongly affect the optimum choice of frequencies.

Table 4

APPROXIMATE PEAK REFLECTION HEIGHTS
FOR STRONG SPE EXAMPLE

Frequency (kHz)	z_R [Eq. (38)] (km)
4	40.7
6	41.8
9	42.8
14	43.9
21	45.0
30	45.9
48	47.1

In practice, we selected the frequency spacing for the strong SPE model by (1) using arbitrarily spaced frequencies to construct a preliminary profile, (2) making an exponential fit to this preliminary profile, and (3) using Eq. (38) to select logarithmically spaced frequencies corresponding to evenly spaced z_R.

Height-Gain Function

It is desirable to have a method of assessing profiles as they are being constructed. We have found the height-gain function H(z) to be useful in this regard. Here we normalize H so that--below the ionosphere--it equals the upgoing wave, which is normalized to unity at the ground. The resulting expression is (Field, Lewinstein, and Dore [1976])

$$H = \left| \frac{1 + R(0)}{1 + R(z)} \exp\left[-i \frac{\omega}{c} \int_0^z dz' \frac{n^2(z')}{A(z')} \right] \right| , \qquad (39)$$

where R(z) is the reflection coefficient and A(z) is the admittance

$$A(z) = \frac{1 + R(z)}{1 - R(z)} \frac{1}{C} .$$

Figure 7a shows H(z) for frequencies of 4 and 48 kHz and the exponential fit to the strong SPE [Eq. (26)]. Comparison with Fig. 6 shows that most reflections occur in the height range where $0.5 \lesssim H(z) \leq 1$. At lower altitudes the ionosphere is too rarefied to reflect the wave strongly; at higher altitudes the signal is so weak that the return is small even if the reflectivity is high. The shaded region thus indicates where both the signal *and* the reflectivity are strong. Figure 7b shows H for the calculated profile, which we have assumed retains its 49-km value at greater altitudes. Again, we see that $0.5 \lesssim H \lesssim 1$ provides a measure of the height range over which the calculated profile is valid; viz., between about 40 and 50 km. Computing H during profile construction gives a criterion for terminating the iterations. When the major contribution for an iteration falls outside the height range defined by $0.5 \lesssim H \lesssim 1$, we have done as well as possible and accept that profile as the final one.

MODEL C-LAYER

The above example pertains to conditions where the conductivity increases monotonically with height. We now consider a qualitatively different situation, where the lower ionosphere exhibits a well-defined layer. Specifically, we used the model given in Fig. 8 (dashed lines), which was shown by Rasmussen, Kossey, and Lewis [1980] to give close agreement between measured and calculated ionosound returns. This profile consists of a sharply bounded layer of conductivity 1.8×10^{-7} mhos/m extending from 63 to 69 km.

The magnitudes of the reflection coefficients were measured at an incidence angle of about 64 deg by Rasmussen, Kossey, and Lewis, and were input to our algorithm at 10 evenly spaced frequencies* between 5 and 50 kHz. Since no phase measurements are available, we had to manufacture phase "data" by integrating Eq. (2) to find Arg R(0) for the "true" profile in Fig. 8. We used the weighting function given by Eq. (26) with $\gamma = 0.5$ km^{-1} and b = 50 km; and, as before, we used a null ($\sigma^0 = 0$) initial profile and a three-point smoothing filter.

*The logarithmic spacing discussed above is not suitable for the type of profile being considered here.

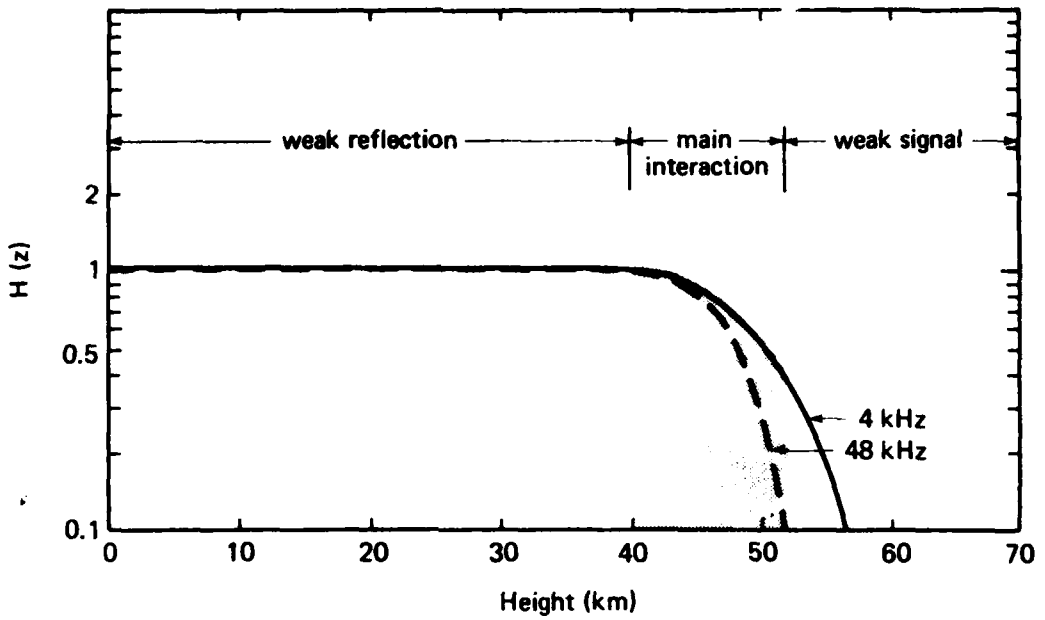

(a) Exponential fit [Eq.(26)]

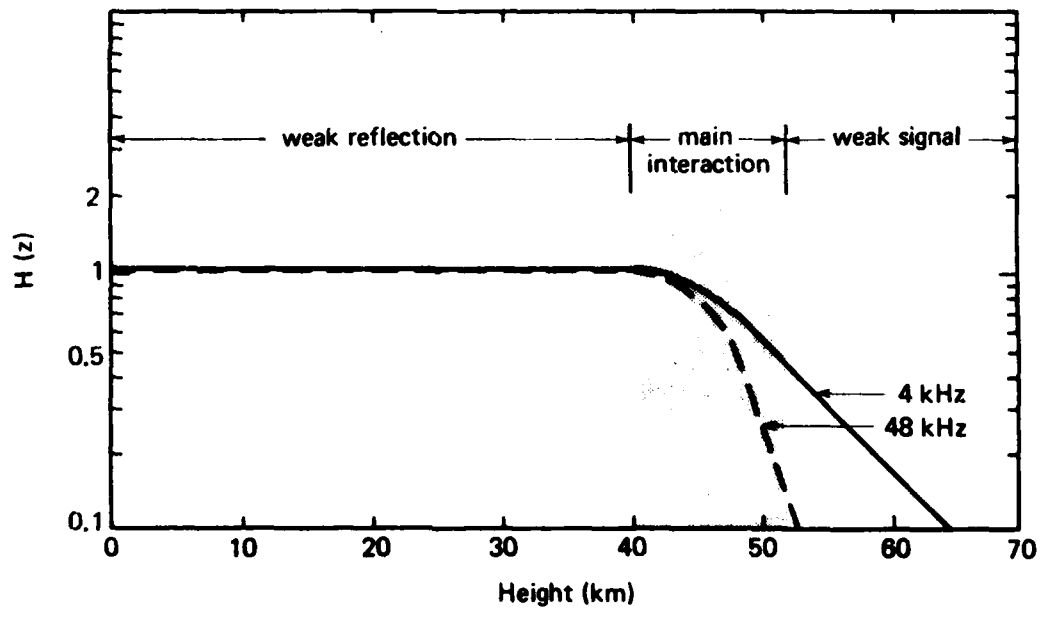

(b) Calculated profile (Fig. 3)

Fig. 7--Normalized height-gain function for (a) true and (b) calculated profiles

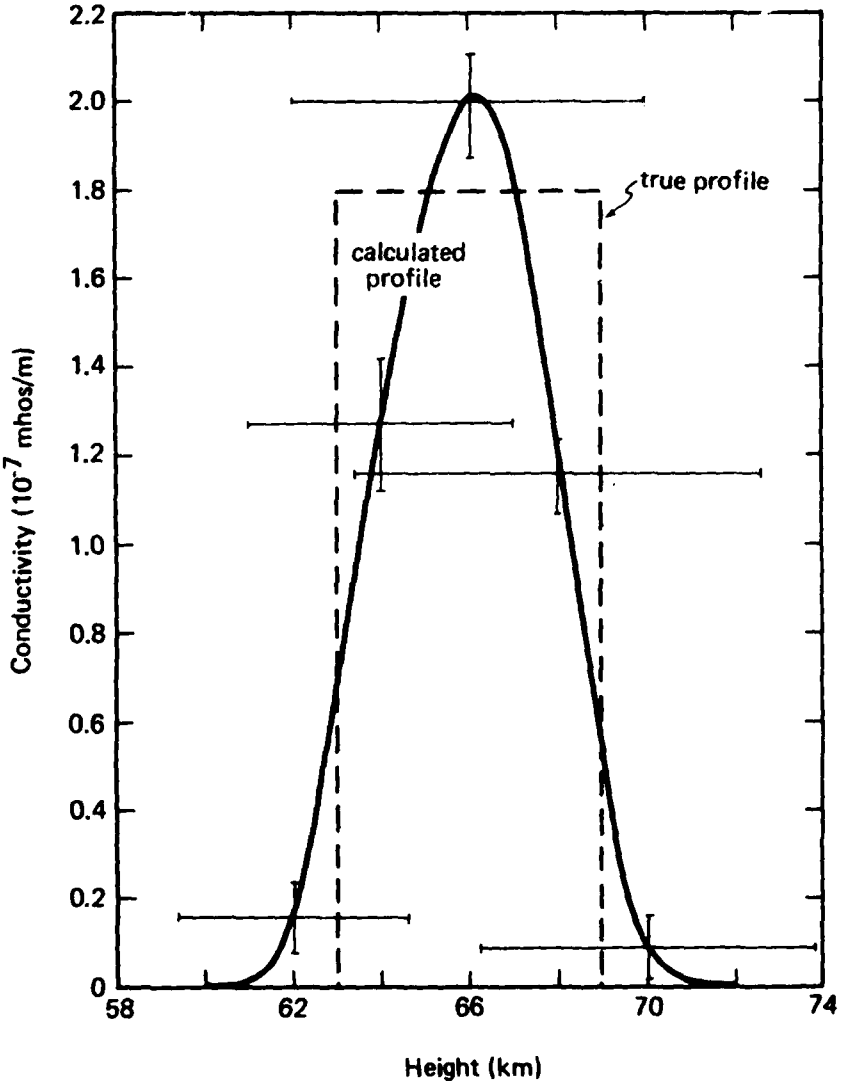

Fig. 8--Calculated and true profiles after 20 iterations for the C-layer example. Vertical bars show uncertainty caused by hypothetical noise in the reflection coefficients. Horizontal bars show uncertainty caused by incompleteness of the reflection data.

Figure 8 shows the profile calculated from the above reflection data after 20 iterations. The calculated and true profiles agree well, particularly with regard to the peak conductivity and location of the layer. The failure of the inverse solution to reproduce the sharp boundaries is caused by the limited height resolution achievable with incomplete data.

To examine the effects of measurement noise on the variance of the computed profile, we use the uncertainties in reflection coefficients given in Table 5. As before, these values are representative of actual measurement uncertainties. The tradeoff between variance and height resolution at a height of 66 km is shown in Fig. 9 for the calculated profile after 20 iterations. The averaging functions for $k < 4$ did not display well-defined peaks, so their widths could not be determined.

Table 5

ASSUMED UNCERTAINTIES IN REFLECTION COEFFICIENTS FOR THE C-LAYER EXAMPLE

Frequency (kHz)	$\lvert S_i/R_i(0)\rvert$
5	0.3
10	0.25
15	0.18
20	0.15
25	0.1
30	0.1
35	0.1
40	0.1
45	0.15
50	0.15

The vertical and horizontal bars on Fig. 8 correspond to the uncertainties caused by noise ($[\mathrm{Var}\ (\sigma)]^{1/2}$) and incomplete data (height resolution) with $k = 8$. Note that the agreement between the calculated and true profiles is much closer than indicated by the

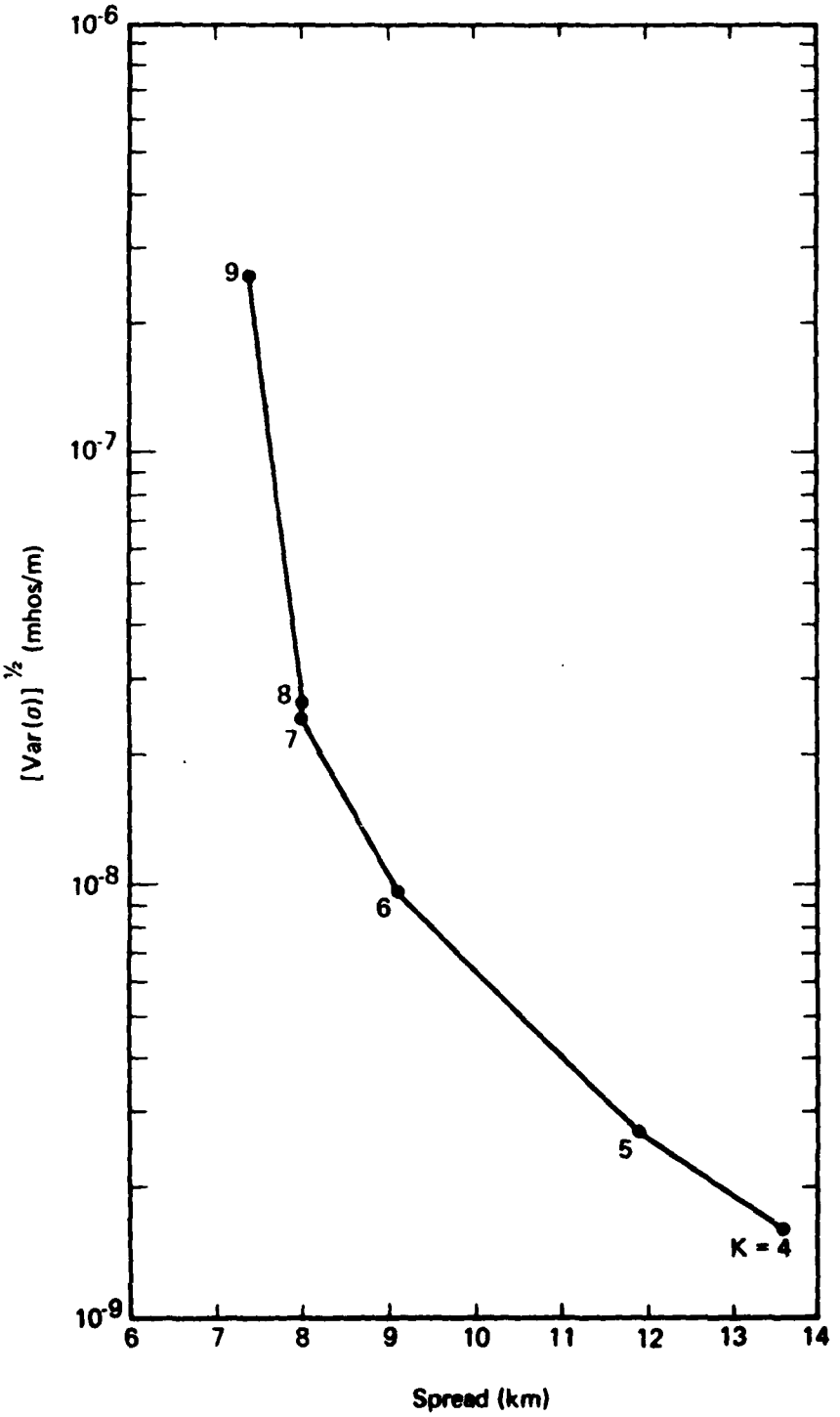

Fig. 9--Tradeoff between height resolution and noise-induced variance for the C-layer example

horizontal bars. This agreement suggests that the height resolution is, in fact, far better than the width of the averaging function A. Shellman [1973] also concluded that this theoretical estimate of height resolution is, in many cases, much too pessimistic. In practice, the achievable resolution is probably best determined by exercising our inversion algorithm for a number of generic profiles, such as the two examples given above.

IV. CONCLUSIONS

Our extension of the Backus-Gilbert theory appears well suited for inferring ionospheric properties from ground-level VLF/LF ionosound data. It permits height profiles of ionospheric parameters to be determined without resorting to trial and error and explicitly gives the relationship between uncertainties caused by noisy and incomplete data. The analyst can therefore choose the best compromise between variance and height resolution of calculated profiles.

We consider only altitudes below about 70 km, where the propagation can be assumed isotropic. This altitude restriction limits application to certain ambient daytime or disturbed conditions. Moreover, only the profile for total conductivity can be found from the reflection data. Determination of profiles for the density and collision frequency of each charged constituent requires auxiliary information. The method can be extended to include geomagnetic effects.

The versatility of our approach is evidenced by its satisfactory performance for two qualitatively different examples--a strong SPE where the conductivity increases quasi-exponentially with altitude and a model C-layer exhibiting a well-defined conductivity peak. In each example, the iterative solution converges toward the true profile despite our use of initial estimates that contain no information about ionospheric structure. The nonlinear relationship between reflection coefficients and ionospheric conductivity apparently causes no difficulties with uniqueness.

We found the height resolution of the calculated profiles for the two examples to be much better than predicted by theory. Other investigators also have reported that the theoretical limit on height resolution is often too pessimistic. The resolution achievable in practice is best determined empirically by inverting computer-generated reflection coefficients for model conductivity profiles that correspond to generic ionospheric conditions.

Ground-level reflection data contain information about only those heights from which significant energy is returned. Our calculated

profiles therefore agree with the true profiles only over a limited height range, which corresponds to the region where the most significant reflections occur. This reflection-height region provides a physical basis for judging where (a) the calculated profiles are reliable, or (b) the interaction between the ionosound signal and the ionosphere is too weak to permit a valid inverse solution.

REFERENCES

Backus, G., and F. Gilbert, "Numerical Applications of a Formalism for Geophysical Inverse Problems," *Geophys. J. R. Astr. Soc.*, Vol. 13, 1967, pp. 247-276.

-----, "The Resolving Power of Gross Earth Data," *Geophys. J. R. Astr. Soc.*, Vol. 16, 1968, pp. 169-205.

-----, "Uniqueness in the Inversion of Inaccurate Gross Earth Data," *Phil. Trans. R. Soc. A*, Vol. 266, 1970, pp. 123-192.

Budden, K. G., *Radio Waves in the Ionosphere*, Cambridge University Press, 1961.

Chuang, S. L., and K. C. Yeh, "A Method for Inverting Oblique Sounding Data in the Ionosphere," *Radio Sci.*, Vol. 12, 1977, pp. 135-140.

Field, E. C., and R. D. Engel, "The Detection of Daytime Nuclear Bursts Below 150 km by Prompt VLF Phase Anomalies," *PROC. IEEE*, Vol. 53, 1965, pp. 2009-2017.

Field, E. C., M. Lewinstein, and M. A. Dore, *Effects of Antenna Elevation and Inclination of VLF/LF Signal Structure*, Pacific-Sierra Research Corporation, Report RADC-TR-76-375, December 1976.

Field, E. C., and M. Lewinstein, *Analysis of Electron Density-Profiles in the Lower Ionosphere*, Pacific-Sierra Research Corporation, Report RADC-TR-78-79, March 1978.

Gilbert, F., "Ranking and Winnowing Gross Earth Data for Inversion and Resolution," *Geophys. J. R. Astr. Soc.*, Vol. 23, 1971 pp. 125-128.

Jackson, D. D., "Interpretation of Inaccurate, Insufficient and Inconsistent Data," *Geophys. J. R. Astr. Soc.*, Vol. 28, 1972, pp. 97-109.

Jupp, D. L. B., and K. Vozoff, "Stable Iterative Methods for the Inversion of Geophysical Data," *Geophys. J. R. Astr. Soc.*, Vol. 42, 1975, pp. 957-976.

Morfitt, D. G., and C. H. Shellman, *A Technique for Obtaining D-Region Electron Density Profiles from VLF Reflection Coefficients*, Naval Ocean Systems Center, Report 781, November 1977.

Oldenburg, D. W., "The Interpretation of Direct Current Resistivity Measurements," *Geophys.*, Vol. 43, 1978, pp. 610-625.

Parker, R. L., "Understanding Inverse Theory," *Ann. Rev. Earth Planet. Sci.*, Vol. 5, 1977, pp. 35-64.

Rasmussen, J. E., private communication, 1981.

Ramussen, J. E., P. A. Kossey, and E. A. Lewis, "Evidence of an Ionospheric Reflecting Layer Below the Classical D Region," *J. Geophys. Res.*, Vol. 85, 1980, pp. 3037-3044.

Reagan, J., Lockheed Palo Alto Research Laboratory, private communication, 17 March 1978.

Shellman, C. H., *Determination of D-Region Electron-Density Distributions from Radio Propagation Data*, Naval Electronics Laboratory Center, NELC/TR 1856, January 1973.

Wiggins, R. A., "The General Linear Inverse Problem: Implication of Surface Waves and Free Oscillations for Earth Structure," *Rev. Geophys. Space Phys.*, Vol. 10, 1972, pp. 251-285.

Appendix

THE SPECTRAL EXPANSION METHOD

Although the inverse solution and its interpretation can be carried out entirely in terms of Fréchet kernels $G_i(z)$ as discussed in Sec. II, significant advantages result from using the set of basis functions formed by orthogonalizing the set $\{G_i(z)\}$. These advantages include (1) improved numerical stability in the iterative inverse solution, (2) the ability to construct resolution functions that are direct generalizations of Dirichlet kernels for Fourier series, and (3) explicit presentation of the tradeoff between achieving high resolution and minimum noise-induced errors. Our analysis has been guided by Parker's [1977] review, which was based in turn on work of Gilbert [1971], Jackson [1972], Wiggins [1972], and Jupp and Vozoff [1975].

The first-order variation in the reflection coefficient $\delta R_i(0)$ at frequency f_i, due to a small change in $\delta\sigma$, is given by Eq. (11), from which it follows that

$$\frac{\delta R_i(0)}{S_i} = \int_0^{z_m} dz \, \frac{G_i(z)}{S_i} \, \delta\sigma(z) \ , \tag{A.1}$$

where S_i represents the measurement uncertainty in $R_i(0)$. Following Oldenburg [1978] and Parker [1977] we slightly generalize the matrix $\underset{\sim}{\Gamma}$ given by Eq. (16) by including the weighting function $w(z)$ and the error estimates S_i:

$$\Gamma_{ij} = \int_0^{z_m} dz \, \frac{G_i(z)}{S_i} \, \frac{G_j^*(z)}{S_j^*} \, [w(z)]^2 \ . \tag{A.2}$$

The use of $w(z)$ allows us to emphasize height regions where significant conductivity is anticipated, and suppress the nonphysical build-up of

conductivity at low heights. By construction $\underset{\sim}{\Gamma}$ is a Hermitian, positive-definite matrix and can therefore be diagonalized by a unitary matrix $\underset{\sim}{U}$ as

$$\underset{\sim}{U}^{\dagger}\ \underset{\sim}{\Gamma}\ \underset{\sim}{U} = \underset{\sim}{\Lambda}\ , \tag{A.3}$$

where $(\underset{\sim}{\Lambda})_{ij} = \lambda_j \delta_{ij}$. Next, we define the function $H_i(z)$ as

$$H_i(z) \equiv \lambda_i^{-1/2} \sum_j (U^{\dagger})_{ij} \frac{G_j(z)}{S_j} w(z)\ . \tag{A.4}$$

The set $\{H_i(z)\}$ is orthonormal since

$$\int_0^{z_m} dz\ H_i(z)H_j^*(z) = \lambda_i^{-1/2}\ \lambda_j^{-1/2} \sum_{k,\ell} (U^{\dagger})_{ik}$$

$$\times \int_0^{z_m} dz\ \frac{G_k(z)}{S_k} \frac{G_\ell^*(z)}{S_\ell^*} [w(z)]^2\ U_{\ell j}$$

$$= \lambda_i^{-1/2}\ \lambda_j^{-1/2} \sum_{k,\ell} (U^{\dagger})_{ik}\ \Gamma_{k\ell} U_{\ell j}$$

$$= \lambda_i^{-1/2}\ \lambda_j^{-1/2}\ \lambda_i \delta_{ij} = \delta_{ij}\ . \tag{A.5}$$

The orthonormality allows the conductivity correction $\delta\sigma(z)$ to be expanded as

$$\delta\sigma(z) = \sum_{i=1}^{n} a_i H_i^*(z) w(z) + \delta\hat{\sigma}(z)\ , \tag{A.6}$$

where

$$a_i = \int_0^{z_m} dz\, H_i(z)\, \frac{\delta\sigma(z)}{w(z)}$$

$$= \lambda_i^{-1/2} \sum_j (U^\dagger)_{ij} \int_0^{z_m} dz\, \frac{G_j(z)}{S_j}\, \delta\sigma(z)$$

$$= \lambda_i^{-1/2} \sum_j (U^\dagger)_{ij}\, \frac{\delta R_j(0)}{S_j} \qquad \text{(A.7)}$$

and $\delta\hat{\sigma}(z)$ is any function orthogonal to the finite set $\{H_i\}$. Equations (A.6) and (A.7) provide the means of computing the correction to the conductivity at each iteration by taking

$$\delta R_i^N = R_i^{data} - R_i^{N-1} \; . \qquad \text{(A.8)}$$

One advantage to finding $\delta\sigma$ in this diagonalized basis is that possible numerical instabilities in computing $\underset{\sim}{\Gamma}^{-1}$, which is needed in the nondiagonal solution, are avoided.

The spectral expansion leads to a simple method of estimating the effect of uncertainties in the measured reflection coefficients on the inferred conductivity profile. Equations (A.6) and (A.7) relate the effect of small variations in the ground-level reflection coefficients on the conductivity at height z. Equivalently these equations may be interpreted as the uncertainty in conductivity due to uncertainties in the data. The variance in conductivity then becomes

$$\text{Var}\,[\sigma(z)] = [w(z)]^2 \sum_{i,j}^{n} \langle a_i\, a_j^* \rangle H_i^*(z) H_j(z) \; , \qquad \text{(A.9)}$$

with

$$\langle a_i \, a_j^* \rangle = \lambda_i^{-1/2} \, \lambda_j^{-1/2} \sum_{k,\ell} (U^\dagger)_{ik} U_{\ell j} \left\langle \frac{\delta R_k}{S_k} \frac{\delta R_\ell^*}{S_\ell^*} \right\rangle , \qquad (A.10)$$

where the $\langle \; \rangle$ denote ensemble averages. Because S_i are the standard deviations in the data and the noise is assumed to be uncorrelated, the covariance matrix for the data is simply

$$\left\langle \frac{\delta R_k}{S_k} \frac{\delta R_\ell^*}{S_\ell^*} \right\rangle = \delta_{k\ell} \qquad (A.11)$$

and the unitarity of U gives

$$\langle a_i \, a_j^* \rangle = \frac{1}{\lambda_i} \delta_{ij} \; . \qquad (A.12)$$

Substitution into Eq. (A.9) produces

$$\text{Var} \; [\sigma(z)] = [w(z)]^2 \sum_i \frac{1}{\lambda_i} \; |H_i(z)|^2 \; . \qquad (A.13)$$

Equation (A.12) states that the expansion coefficients a_i are statistically independent and have variance $1/\lambda_i$, where λ_i are the positive-definite eigenvalues of the Γ matrix. The spectral expansion [Eq. (A.6)] can therefore be interpreted as a superposition of terms having progressively greater statistical uncertainty. The diagonalization process recombines the original Fréchet kernels G_i to produce components H_i, which allow the conductivity features that can most reliably be inferred from the data to be identified. In practice, a large reduction in Var (σ) can be achieved by suppressing a few of the smallest eigenvalue terms from Eq. (A.6). Because eigenvalue components with large λ_i tend to be smoother than those with small λ_i, this truncation removes the highly oscillatory terms, which

are typically the noisiest in the data set. This filtering capability is not possible in the undiagonalized basis set.

The resolution analysis treated in Sec. II can be assily carried out in the diagonalized basis. Denoting by $\langle \delta\sigma(z) \rangle$ the estimate of $\delta\sigma(z)$ produced by retaining $k \leq n$ terms in the spectral expansion [Eq. (A.6)], we find

$$\langle \delta\sigma(z) \rangle = w(z) \sum_{i=1}^{k} a_i H_i^*(z)$$

$$= \int_0^{z_m} dz' \, \delta\sigma(z') \, \frac{w(z)}{w(z')} \sum_{i=1}^{k} H_i^*(z) H_i(z')$$

$$\equiv \int_0^{z_m} dz' \, \delta\sigma(z') A(z, z') \, . \qquad \text{(A.14)}$$

The averaging function A has the same form as the Fourier series Dirichlet kernel discussed in Sec. II. Its width is a measure of the maximum height range over which the conductivity profile could--in principle--be deformed and still be consistent with the reflection-coefficient data set. In practice, we have found that the height resolution is better than indicated by this conservative criterion.

In general, retaining fewer terms in Eq. (A.14) has the effect of increasing the width of the averaging function. Because this process also decreases the variance in the conductivity [see Eq. (A.13)] there is a tradeoff between high resolution and statistical reliability. Our experience indicates that dropping the smallest eigenvalue terms produces a significant improvement in estimated variance, while causing only a negligible degradation in height resolution. This behavior is illustrated by the examples in Sec. III.

MISSION
of
Rome Air Development Center

RADC plans and executes research, development, test and selected acquisition programs in support of Command, Control Communications and Intelligence (C^3I) activities. Technical and engineering support within areas of technical competence is provided to ESD Program Offices (POs) and other ESD elements. The principal technical mission areas are communications, electromagnetic guidance and control, surveillance of ground and aerospace objects, intelligence data collection and handling, information system technology, ionospheric propagation, solid state sciences, microwave physics and electronic reliability, maintainability and compatibility.

Printed by
United States Air Force
Hanscom AFB, Mass. 01731

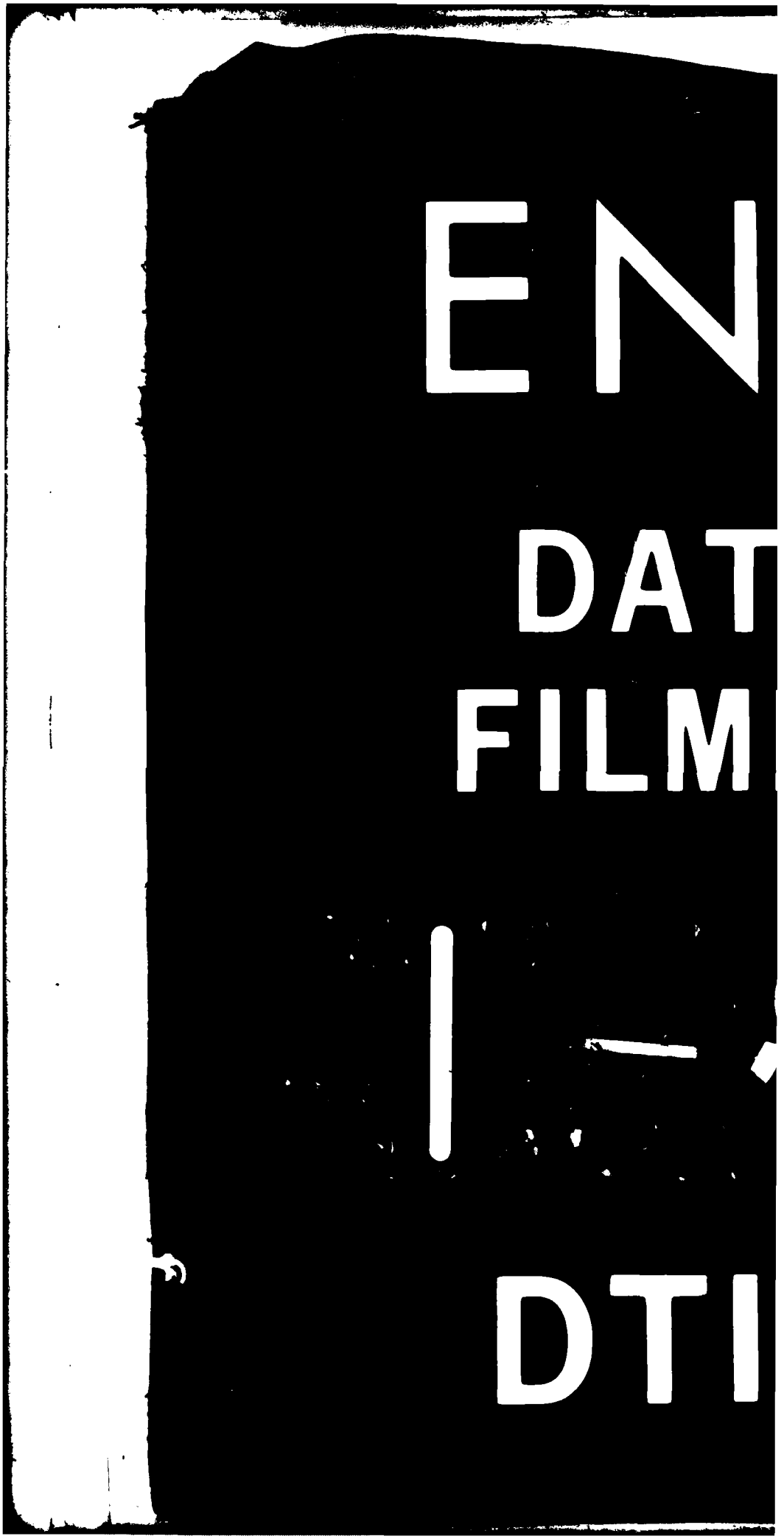
EN
DAT
FILM
DTI